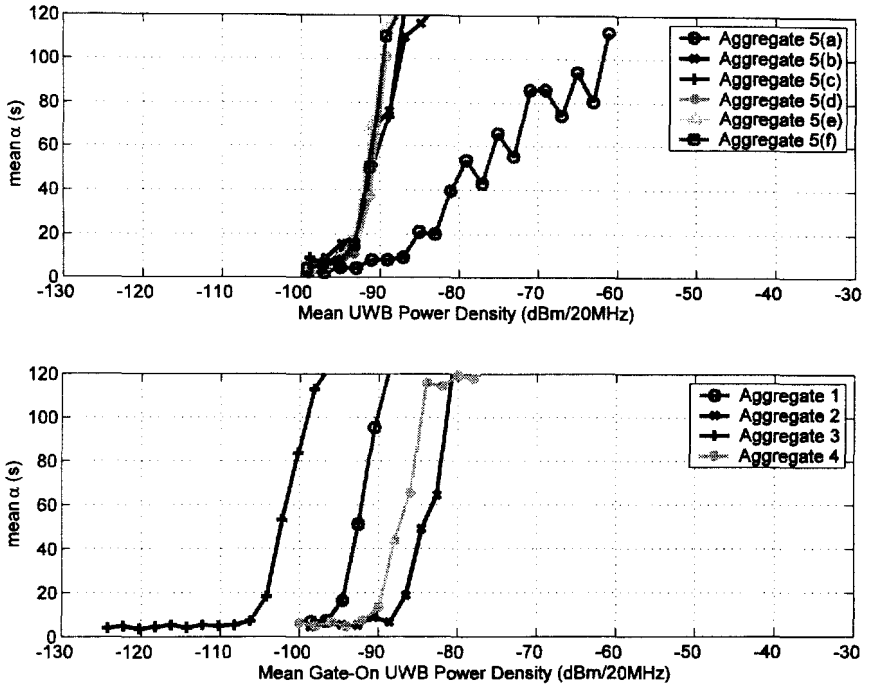

Figure 6.2.11. RQT of Rx 1 when exposed to aggregate UWB interference.

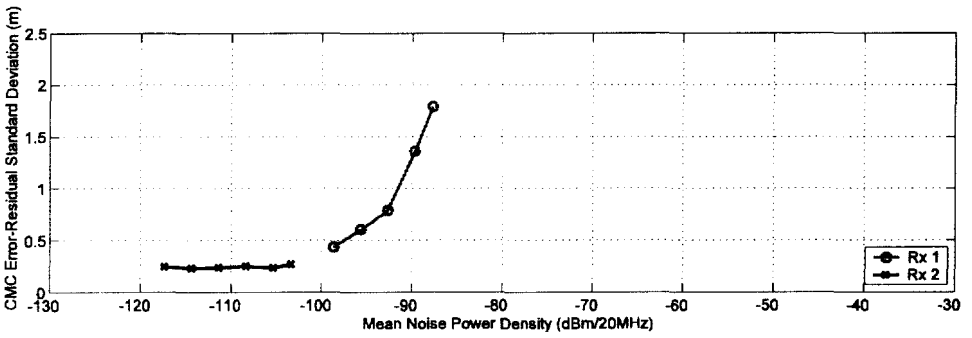

Figure 6.2.12. PSR accuracy of GPS receivers when exposed to Gaussian-noise interference.

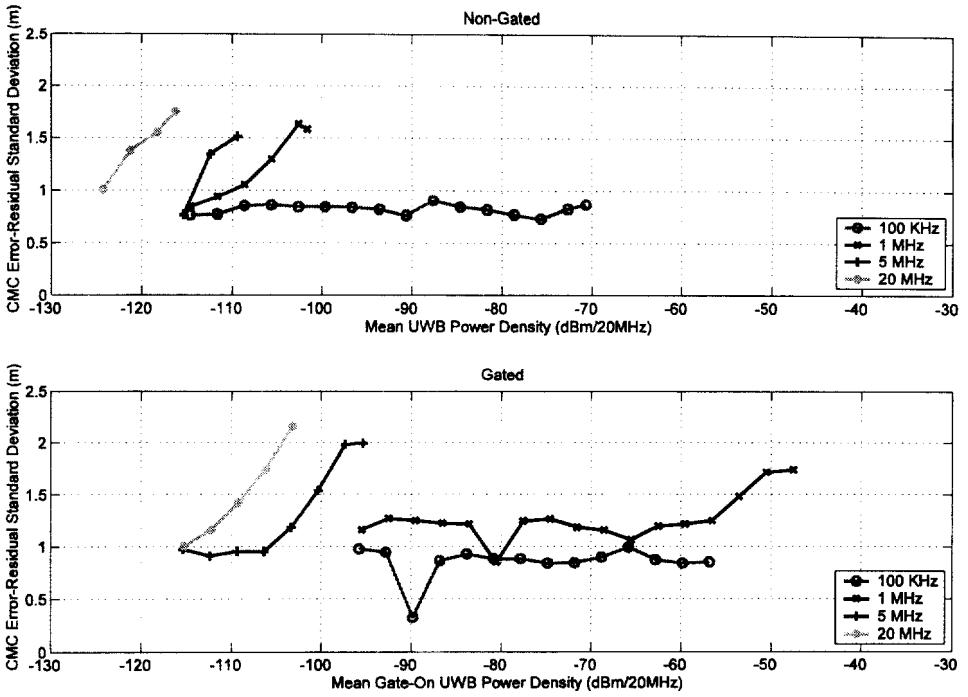

Figure 6.2.13. PSR accuracy of Rx 1 when exposed to UPS UWB interference.

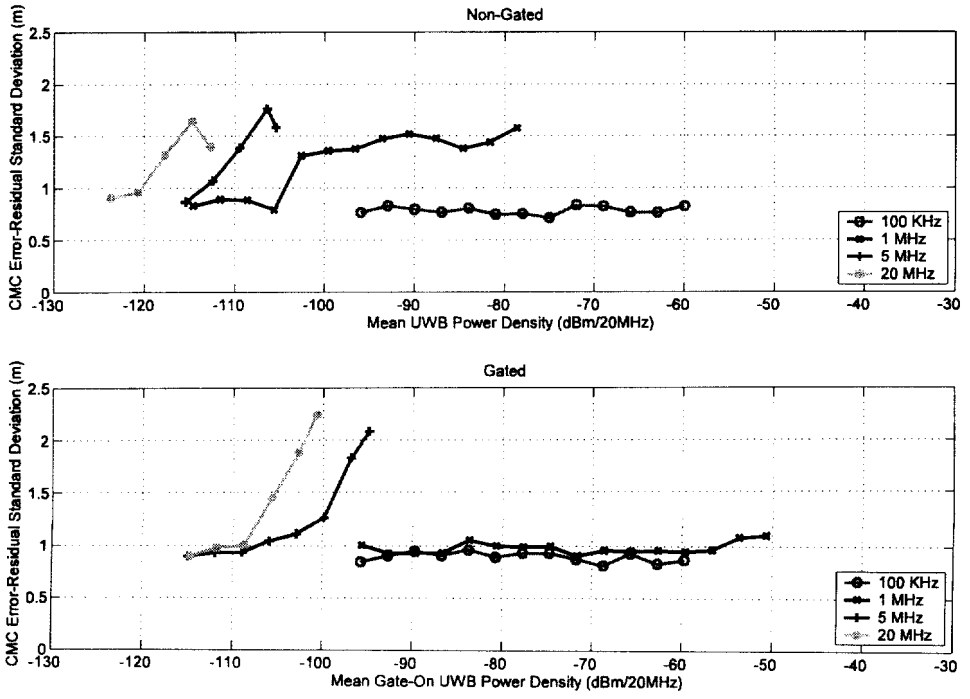

Figure 6.2.14. PSR accuracy of Rx 1 when exposed to OOK UWB interference.

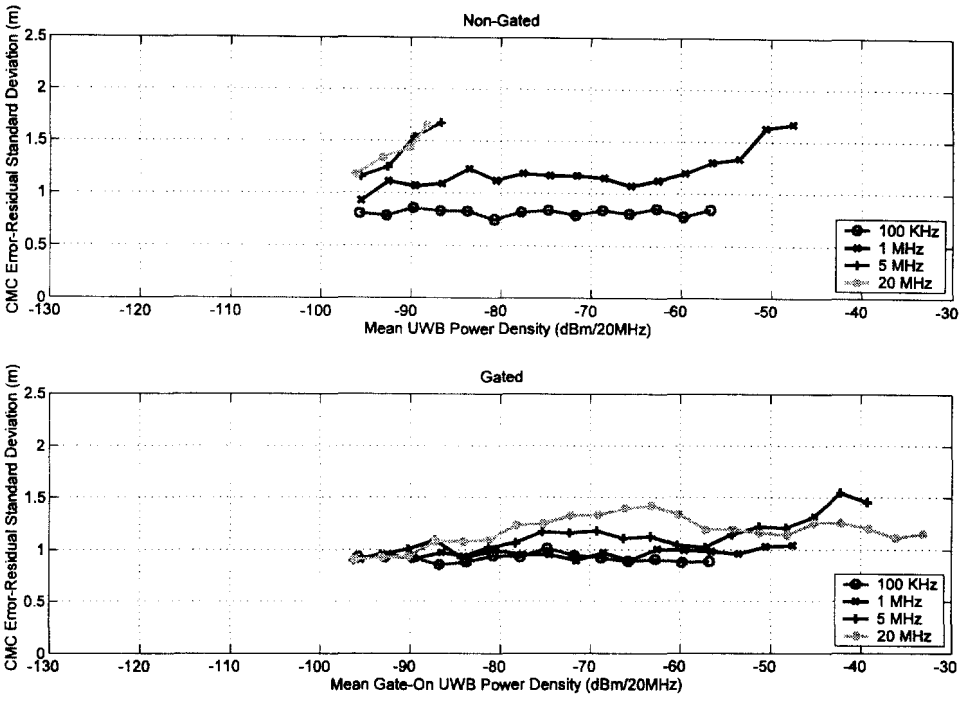

Figure 6.2.15. PSR accuracy of Rx 1 when exposed to 2%-RRD UWB interference.

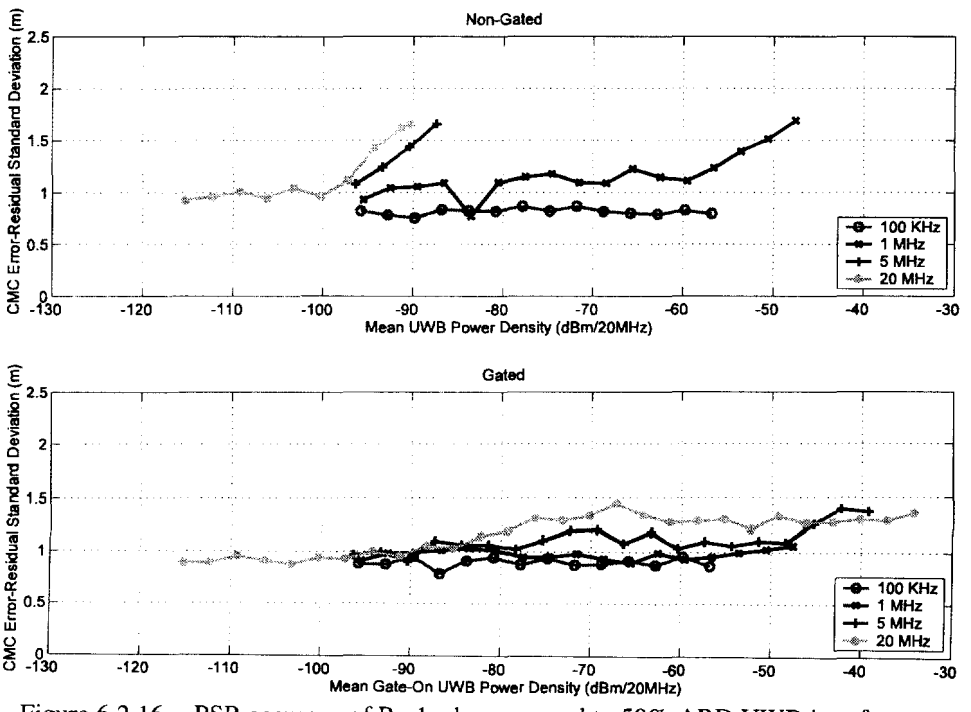

Figure 6.2.16. PSR accuracy of Rx 1 when exposed to 50%-ARD UWB interference.

6.3 Summary of Measurement Results

Because of the different receiver bandwidths and different signal processing techniques employed, each receiver responds in a different manner. In addition, there are certain trends in receiver response to UWB interference which can be identified and related to various characteristics of the UWB signals. In this section, these trends will be summarized for both receiver differences and variation in UWB signal interference.

6.3.1 Receiver Observations

Receiver 1 is a general purpose navigation receiver. Receiver 2 is a high-precision, semi-codeless receiver which relies heavily upon carrier phase information. It also has narrow correlator capabilities, and therefore wide bandwidths. It should be noted that Rx 2 was tested without the Gaussian-noise source, except for the Gaussian-noise interference test.

Several general observations can be made with respect to each receiver:

1. Figures 6.2.1 through 6.2.4 show that Rx 1 BL points occur at higher UWB signal powers for ARD and RRD, and Rx 2 showed BL at higher UWB signal powers for OOK and UPS.
2. As exemplified in Figure 6.2.6 and throughout the RQT results (e.g., Figures 6.2.7 through 6.2.10), the same RQT generally occurs at a higher interference power for Rx 1 than Rx 2.
3. Figures F.2.1 through F.2.33 show that Rx 1 is much more tolerant of cycle-slip conditions.
4. For most of the lower PRF cases (1-MHz and 0.1-MHz PRF), Rx 1 reported no change in C/N_0 despite the fact that UWB interference power was as much as 50 dB above the added Gaussian noise. This was also seen for Rx 2 for all UWB signal power levels and types.
5. Sometimes the receivers were able to reacquire at UWB signal power levels greater than the BL point (see Figures F.1.36, F.2.1, F.2.10 through F.2.15, F.2.18, F.2.19, F.2.21, F.2.22). This occurred more frequently with Rx 2.

From these and other observations, several conclusions can be drawn:

1. Because of its intended application, BL occurred for Rx 2 whenever there are cycle slips.
2. BL results show that Rx 2 is more tolerant of interference with spectral lines.
3. Reacquisition can sometimes occur at UWB power levels greater than the BL point for two reasons. One reason is that the BL point is probabilistic and can occur over a range of power levels from one time to the next. The other reason is that BL measurement duration is long, while maximum RQT is relatively short.
4. For Rx 1, the observational results are correlated to BL and RQT. For many of the UWB signals, CMC, ADR, cycles slips, and C/N_0 show significant changes and parellel RQT as the UWB interference power levels approached the BL point. However, for Rx 2 only RQT showed change prior to the BL point.

4. RQT has been found to be the most sensitive parameter for identifying interference effects on the receiver. In fact, sometimes RQT is elevated when UWB power levels are as much as 10 to 20 dB below the BL point (see Figures F.1.19, F.1.20, F.1.22, F.1.27, F.1.30, F.1.38, F.1.39, and F.2.20).

6.3.2 Variations Due to UWB Signal Characteristics

Aside from receiver differences, there are trends in receiver response related to the characteristics of the UWB signals themselves, such as pulse spacing, PRF, gating, and the accumulation of multiple UWB signals.

Pulse Spacing

Receiver effects can be directly related to the different modes of pulse spacing – UPS, dithering, and OOK. Any time the UWB signal has a uniform pulse spacing, there are spectral lines, and when these spectral lines lie within the GPS band, there is potential for alignment with spectral lines of the GPS signal. This alignment is particularly invasive as evidenced by BL at low UWB powers in Figures 6.2.1 and 6.2.2. Particularly for higher PRFs, where more power is gathered up into each of the spectral lines, Rx 1 breaks lock at power levels as much as 25 dB below the added noise. The same trends can be seen for CMC and ADR error-residual, and cycle slips.

On-off-keying, since it too has spectral lines, can have a significant impact on GPS receivers. This is evident in Figures 6.2.1, and 6.2.2, where for higher PRFs the BL point occurs by as much as 20 dB below the added noise. However, the effects of OOK are less detrimental than for UPS; this is because the spectral power is distributed between spectral lines and a noise component (see Appendix D). Also, as evidenced by comparing UPS with OOK in the APDs, OOK has the effect of increasing the peak-to-average noise power and decreasing the percentage of time the signal is present above the system noise, thus decreasing the impact on receiver performance.

Dithering reduces the impact of UWB interference on GPS receivers. As discussed in Section 4.1.2, dithering can reduce or eliminate spectral lines – thus spreading the power over the band and reducing the effects of interference. As evidenced by APDs such as those shown in Figures C.3.10 and C.3.12, UWB signals at high PRF rates (e.g., 5 and 20 MHz) are distributed similarly to Gaussian noise when limited to a 3-MHz bandwidth. This is in keeping with the BL results shown in Figures 6.2.1 through 6.2.4, where for higher PRFs, dithering shows BL results similar to Gaussian noise. For the lower PRFs of 1.0 and 0.1 MHz, the impact from dithered UWB signals is even further reduced.

Pulse Repetition Frequency

Higher PRFs have a greater detrimental effect for two reasons. One is that for those cases with spectral lines, greater power is gathered into each spectral line. The other reason is that higher PRFs result in a reduced peak to average power ratio and a greater percentage of time for which the signal is present. This is evident in measured APDs such as those shown in Figure C.3.9. For each of the plots in Figures 6.2.1 through 6.2.4, one can see a natural progression of the point of BL moving to lower UWB power densities as the PRF increases, irrespective of the pulse spacing mode. The same trends can be seen for RQT, CMC and ADR error-residual, and cycle slips.

Gating

Gating reduces the impact on receivers for two reasons. One is that, as mentioned in Section 4.1.2, the power of individual spectral lines is spread out into multiple lines, thus reducing the power contained in any single line. The other reason is that, for signals of equal gated-on power density, the percentage of time the signal is present is less with gating. For each of the parameters measured, one can readily see that for the same power density during the gated-on time, the detrimental effects are significantly reduced as compared to non-gated signals.

Accumulation of Multiple UWB Signals

With the aggregate of multiple asynchronous UWB signals, one would expect the sum of the signals to become more Gaussian noise-like in its distribution and effects on GPS receivers. There are several trends which can be noted when examining the characteristics of each of the aggregate scenarios described in Table 4.1.2.2. As shown in Figures C.3.30 and C.3.31, increasing the number of summed signals in scenario 5 causes the aggregate signal to become more Gaussian – the extent being dependent upon the bandwidth. Scenarios 2 and 4 are somewhat more impulsive in nature because of asynchronous gating applied to several of the signals. Scenarios 1 and 3 both have relatively Gaussian distributions; however, scenarios 3 and 4 both have strong spectral lines – scenario 3 being potentially more invasive, in that it has more power gathered up into lines spaced 10 MHz apart.

The characteristics of these aggregate signals can be directly related to the impact on receiver performance. As noted in Figure 6.2.5, scenarios 1 and 4 show BL test results similar to noise. Scenario 2, which is essentially the same as scenario 1 but with gating applied, shows a BL point at a lower gated-on power than its non-gated counterpart. Scenario 3 shows a BL point at a low signal power because, while its APD is Gaussian distributed, it has strong spectral lines (see Figure 6.3.2.1). Scenario 5 (*a* through *f*) shows effects similar to Gaussian noise for an aggregate of anything more than 2 signals.

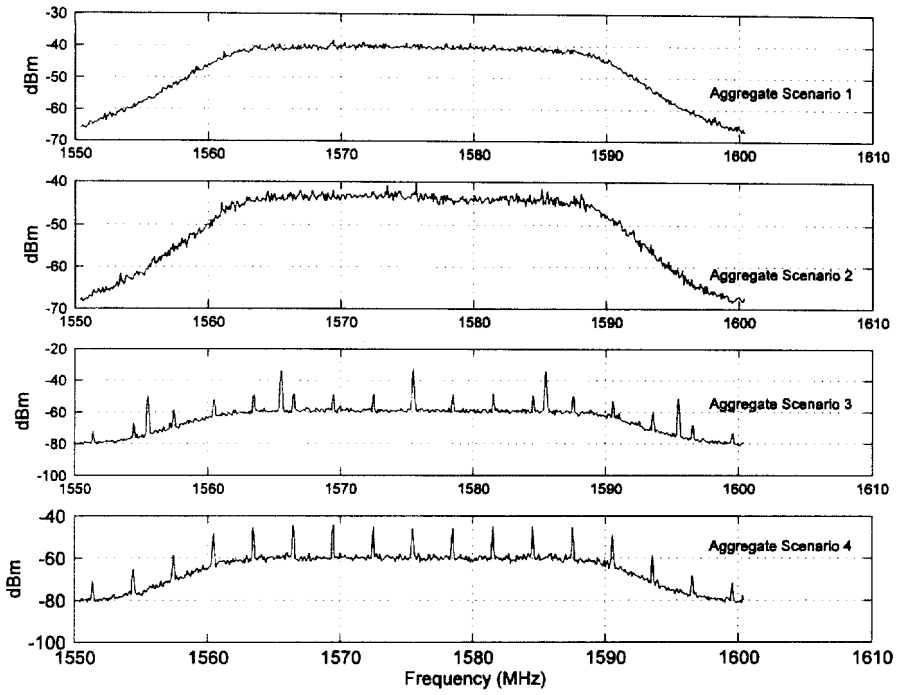

Figure 6.3.2.1. Spectral characteristics (through a 24-MHz filter) for aggregate case 1 through 4.

7. CONCLUSION

Several major studies were performed to evaluate the effect of UWB signals on GPS receiver performance. These studies characterized the UWB signals, compared conducted and radiated UWB signals, and evaluated effects of the UWB interference on GPS receiver operation (i.e. locking) and "observables."

The GPS signal was generated by a GPS constellation simulator. A select group of UWB signals were generated with a programable arbitrary waveform generator and custom hardware which triggered a sequence of UWB pulses. Signals with uniform pulse spacing (UPS), on-off-keying (OOK) , 2% relative reference dithering (RRD), and 50% absolute reference dithering (ARD) signals at 0.1, 1.0, 5.0, and 20.0 MHz pulse repetition frequencies (PRF) were used. These signals could also be gated to imitate the bursty nature of some UWB devices. Various combinations of signals were at times combined to simulate interference from multiple UWB devices.

The UWB signals were sampled and characterized with the amplitude probability distribution (APD) in hopes that APD features (i.e., constant amplitude, Gaussian noise, and impulsive noise) can be correlated to GPS receiver performance degradation. In addition, although under usual conditions, radiated UWB and GPS signals are combined at the antenna, this study uses conducted signals to maximize control and repeatability of experimental conditions. A comparison of radiated and conducted UWB-signal APDs and waveforms showed that systematic errors were not introduced by the conducted approach.

Two independent operational tests, break lock (BL) and reacquisition time (RQT), measured the receiver's ability to maintain and reacquire lock over a range of UWB signal powers. The BL and RQT metrics bracket a region of GPS receiver performance degradation. The RQT determines the lower bound where the interference begins to have a detrimental effect on the operation of the receiver. The BL point sets the upper bound where operation is impossible.

The observational test, conducted in parallel with the BL test, retrieved "observable" measurements made by the GPS receiver to estimate performance degradation. Pseudorange and carrier phase measurements were used to determine various range estimates that were compared to simulated ranges in order to evaluate the effects of UWB interference. Cycle slip indication and signal-to-noise ratio measurements evaluate the receivers ability to detect interference and make decisions regarding GPS measurement integrity.

The BL point varied most with the type of receiver. The semi-codeless receiver broke lock with the first indication of cycle slip conditions. The general purpose navigation receiver continued operation with frequent indications of cycle slip conditions. RQT was found to be the most sensitive metric. In many cases RQT showed increases without attendant degradations in range error or increases in frequency of cycle-slip conditions. RQT, range error, and cycle slip condition indicators generally show a gradual degradation as UWB signal power is increased.

This shows that the strength of the measurement methodology lies not in a single result but in the total picture painted by the combined results.

UPS and OOK signals have discrete spectral lines. Time-varying Doppler shift due to satellite motion inevitably causes these lines to interfere with GPS discrete spectral lines. These test results show that observables degrade at low UWB signal powers as the lines approach and recede. Line interference becomes more severe as PRF increases.

APDs of sampled 50%-ARD and 2%-RRD signals approach that of Gaussian noise as PRF increases. Consequently, for high-PRF dithered signals, interference effects resemble that of Gaussian noise. In general, low-PRF dithered signals generate more impulsive interference which is more benign than Gaussian noise.

8. ACKNOWLEDGMENTS

This investigation required a number of ITS engineers with a broad range of expertise and skills. The authors recognize Dr. William Kissick for his vision and leadership; Yeh Lo, John Ewan, and Wayde Allen for hardware design and production; Robert Matheson for his written contributions and insights shared; Brent Bedford for coordination of the radiated measurements; and Jeanne Ratzloff for web site development.

Steve Jones, Ed Drocella, Mark Settle, and David Anderson of the Office of Spectrum Management contributed significantly in the development of the original test plan and interpretation of the results.

Dr. Robert Johnk of the National Institute of Standards and Technology (NIST) Radio-Frequency Technology Division (Time-Domain Laboratory) is recognized for his efforts in the radiated measurements of UWB signals.

Finally, the authors recognize the 746th Test Squadron from Holloman Air Force Base for engineering support with respect to the GPS simulator.

9. REFERENCES

[1] *Notice of Proposed Rulemaking*, ET Dkt. 98-153 (rel. May 11, 2000), Federal Register, June 14, 2000, vol. 65, No. 115), pp. 37332 - 37335.

[2] W.A. Kissick, Ed., "The temporal and spectral characteristics of ultrawideband signals," NTIA Report 01-383, Jan. 2001.

[3] Recommendation ITU-R M.1477, Technical and Performance Characteristics of Current and Planned RNSS (Space-to-Earth) and ARNS Receivers to be Considered in Interference Studies in the Band 1559-1610 MHz.

[4] ARINC Research Corporation, *Navstar GPS Space Segment/Navigation User Interfaces* (Sept. 25, 1997).

[5] J.L. Leva, M.U. deHaag, and K.V. Dyke, "Performance of Stand Alone GPS," Chapter 7 of *Understanding GPS Principles and Applications*, E.D. Kaplan, Ed., Boston, MA: Artech House, 1996, pp. 237-320.

[6] P.Axelrad and R.G. Brown, "GPS Navigation Algorithms," Chapter 9 of *Global Positioning System: Theory and Applications*, B.W. Parkinson and J.J. Spilker, Eds., Washington, DC: American Institute fo Astronautics, Inc., 1996, pp. 409-433.

[7] O.L.Davies and P.L. Goldsmith, "Averages and Measures of Dispersion", Chapter 3 of *Statistical Methods in Research and Production*, O.L. Davies and P.L. Goldsmith, Eds., Tweeddale Court, Edinburgh: Oliver and Boyd, 1972, pp. 30-57.

[8] J.R. Green and D. Margerison, "Confidence Intervals," Chapter 6 of *Statistical Treatment of Experimental Data*, New York, NY: Elsevier Scientific Publishing, 1978, pp. 93-111.

10. GLOSSARY

ADR	Accumulated delta-range
APD	Amplitude probability distribution
ARD	Absolute referenced dithering
ARL/UT	Applied Research Laboratories of the University of Texas at Austin
AWG	Arbitrary waveform generator
BL	Break-lock
BPF	Bandpass filter
BW	Bandwidth
C/A Code	Coarse acquisition code
CDF	Cumulative distribution function
CDMA	Code division multiple access
CMC	Code-minus-carrier
CW	Continuous wave
DOT	Department of Transportation
DPSR	Delta-PSR
GPS	Global positioning system
FCC	Federal Communications Commission
IF	Intermediate frequency
ITS	Institute for Telecommunication Sciences
L1 band	GPS frequency band centered at 1575.41 MHz

L2 band	GPS frequency band centered at 1227.6 MHz
LNA	Low noise amplifier
LSNB	Line spreading null-to-null bandwidth – referring to the null spacing of the convolving $sinc^2$ function as a result of gating, where the null-to-null bandwidth is equal to 2 times the reciprocal of the gated-on time.
LSS	Line spread spacing – referring to the spacing between lines of the convolving $sinc^2$ function as a result of gating, where the distance between lines is equal to the reciprocal of the gating period
ND	Noise diode
NIST	National Institute for Standards and Technology
NPRM	Notice of proposed rulemaking
NTIA	National Telecommunications and Information Administration
OSM	Office of Spectrum Management
OOK	On-off keying
PDOP	Position dilution of precision
PPM	Pulse-position modulation
PRL	Pattern repetition lines – referring to spectral lines generated due to a repetition of the pulse pattern
PRF	Pulse repetition frequency
PRP	Pulse repetition period – defined as the reciprocal of PRF
PRR	Pulse repetition frequency
PRN	Pseudo-random noise
PSR	Pseudorange
P(Y) code	Encrypted high-precision pseudo-random noise (PRN) codes

RF	Radio frequency
RRD	Relative referenced dithering
RQT	Reacquisition time
RQT_{max}	The maximum time for reacquisition, after which the RQT trial is considered unsuccessful.
Rx	Receiver
SN	Spectral node – referring to a spectral feature due to the placement of the position of pulses within discrete bins
SNR	Signal-to-noise ratiow
SV	Space vehicle
Tx	Transmitter
UPS	Uniform pulse spacing
UWB	Ultrawideband – referring to ultrawideband signals
VA	Variable attenuators

APPENDIX A: CONDUCTED VERSUS RADIATED PATH MEASUREMENTS

A.1 Overview

As illustrated in Figure A.1.1, there are two possible methods for performing radio interference measurements; one is conducted and the other is radiated. While radiated measurements have the advantage of simulating real world conditions, conducted measurements have the distinct advantage of being able to test under highly controlled conditions. The latter were chosen as the preferred method for performing the UWB/GPS interference measurements at the Institute for Telecommunication Sciences (ITS). To impute validity for the measurements, it is imperative, however, that the effects on the signal within the frequency band of interest be nearly identical, whether conducted or radiated. As the UWB signal proceeds from A to B or from A to C (shown in Figure A.1.1), the temporal characteristics of the pulse change due to various effects on the magnitude and phase across the frequency band. Some of this is expected because filtering, attenuation, and amplification occur along the path. The phase and magnitude of the signal are represented by $X(j\omega)$ at the pulse generator output connector, and $Y_1(j\omega)$ and $Y_2(j\omega)$ at the output of the GPS antenna terminal for the radiated path and the output of the LNA for the conducted path respectively (where $X(j\omega)$, $Y_1(j\omega)$, and $Y_2(j\omega)$ are the Fourier transform of the time-domain signal at the respective locations – A, B, and C). The transfer functions of the different paths are represented by $H(j\omega)$ and $G(j\omega)$, whereby $H(j\omega) = Y_1(j\omega) / X(j\omega)$ and $G(j\omega) = Y_2(j\omega) / X(j\omega)$. Ideally, $H(j\omega)$ and $G(j\omega)$ should be identical across the frequency band of interest.

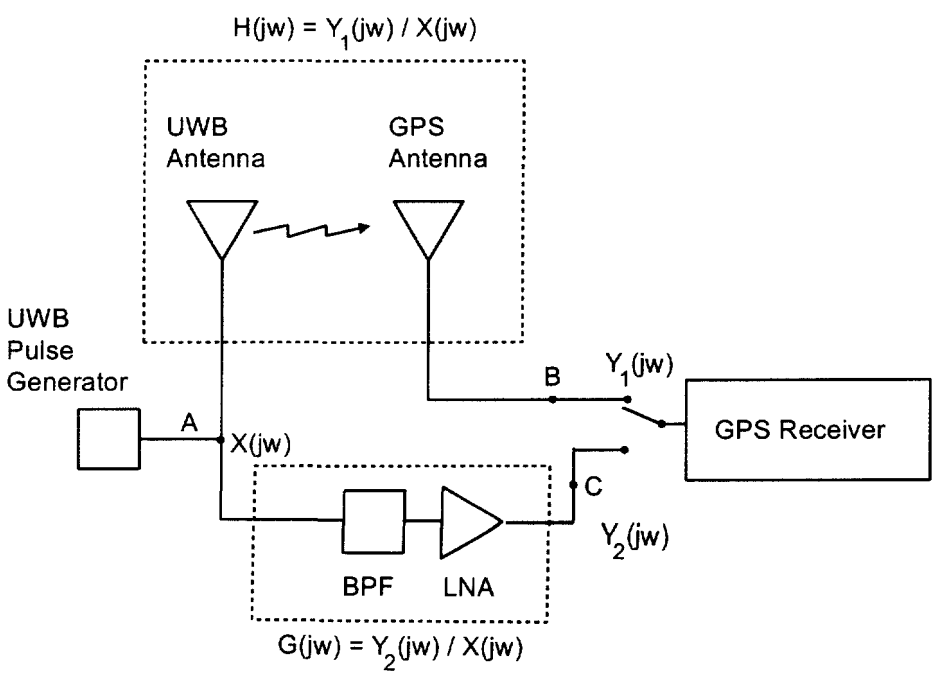

Figure A.1.1. Conducted versus radiated measurement concept.

To help match the transfer functions between the two paths, a band-pass filter (BPF) and low-noise (LNA) amplifier of bandwidth and gain, equivalent to that of the GPS antenna, were placed in the conducted path for all interference measurements. The UWB antenna is assumed to have a much wider bandwidth, making it less likely to contribute to narrowing of the bandwidth and therefore, does not require a filter to emulate its bandwidth characteristics.

Because, in real world applications, both UWB antennas and GPS antennas are used to transmit and receive pulsed or digital signals, it is assumed that the magnitude and phase distortion is minimal over the L1 band, and therefore, there should be little difference in signals (conducted or radiated) as seen in the L1 band. To verify these assumptions, measurements described herein were performed to determine the degree to which signals passed through the two paths, conducted and radiated, are likely to be the same. This was accomplished by measuring temporal characteristics of the UWB signal at points A and B as represented in Figure A.1.1. The measurements include high speed digitization of a single pulse (to determine the transfer function of the radiated path by performing Fourier analysis), as well as multiple pulse acquisitions to compare APD characteristics at points A and B for four different pulse spacing modes.

A.2 Single Pulse Measurement

High speed digitization of UWB signals emitted from a Time Domain Corporation PG-2000 pulse generator was conducted by the National Institute for Standards and Technology (NIST) Radio-Frequency Technology Division in their Time-Domain Laboratory to obtain data that represents the radiated time-domain waveform. The goal of these measurements was to capture a detailed view of a single pulse using a single-event transient digitizer capable of achieving very high sample rates. The digitizer used in this study possesses a bandwidth of 4.5 GHz with a maximum of 1,024 samples in a single shot and is designed to perform high fidelity measurements on a single pulse.

Conducted measurements were performed using the test fixture shown in Figure A.2.1. The RF output of the UWB device-under-test was connected using a coaxial transmission line to an attenuator, used to prevent overloading and damage to the measurement device from an overly strong signal level. The signal was then split into two equal amplitude levels and fed into a trigger port and a signal port on the transient digitizer.

Radiated measurements were performed using the test fixture shown in Figure A.2.2. Data was acquired in the NIST anechoic chamber using two different antennas: a UWB antenna (transmit) supplied by the manufacturer of the pulse generator, and a GPS antenna (receive) supplied with one of the receivers under test. The signal was split into two equal amplitude levels and fed into a trigger port and a signal port on the high speed transient digitizer.

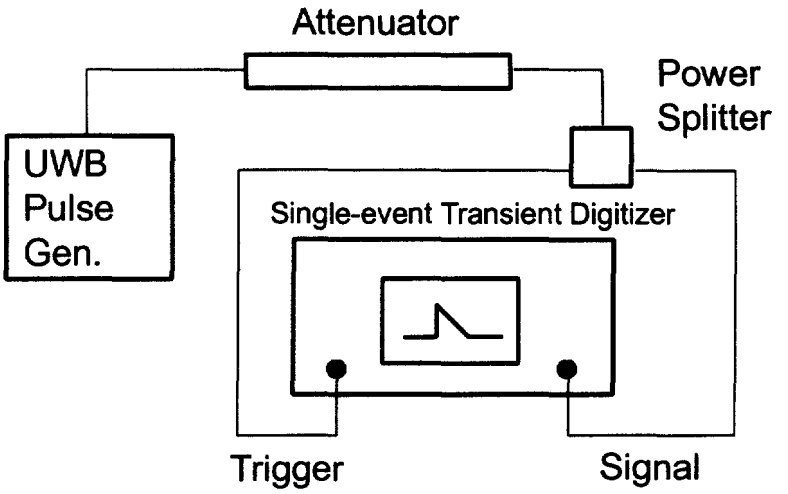

Figure A.2.1 Conducted measurement test setup.

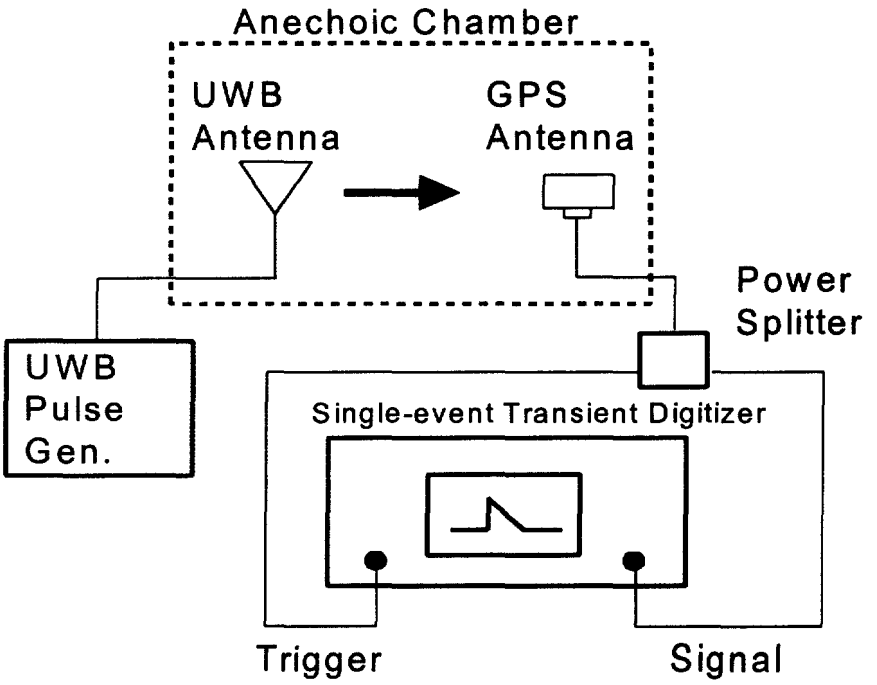

Figure A.2.2. Radiated measurement test setup.

The acquired pulses were processed to derive the complex transfer function for the radiated path ($H(j\omega)$). This was accomplished by performing a Fourier transform on the digitized time-domain radiated and conducted pulses to give $Y_1(j\omega)$ and $X(j\omega)$ respectively. To increase the frequency resolution to 150 kHz, each digitized pulse was padded with zeros (prior to applying the Fourier transform) to give a total sample size of 131,072 points. This is justified by the fact that the pulse goes to zero after full decay, and by padding with zeros, we are adding additional information that we know to be true. The complex transfer function of the radiated path was then determined by dividing $Y_1(j\omega)$ by $X(j\omega)$ to provide magnitude and group delay information across the band of interest. Since the transfer function of path A to C ($G(j\omega)$ in Figure A.1.1) is determined primarily by the inline bandpass filter (used during interference measurements), we can compare the effects of the two different paths by comparing $H(j\omega)$ (the transfer function of the radiated path) with $G(j\omega)$ (the transfer function of the filter). Figures A.2.4 through A.2.13 show the magnitude and group delay for the radiated path and for each of the inline filters used (filters F1 - F4 described in Appendix A). While there are significant differences at wider bandwidths, there is very little difference in the 20-MHz bandwidth centered at L1.

In addition to the magnitude and group delay characteristics, we can further compare the time-domain characteristics of the two different paths (A to B and A to C) by multiplying both $Y_1(j\omega)$, and $Y_2(j\omega)$ by the transfer function of a narrower filter (e.g. a 24-MHz bandpass filter) and applying the inverse Fourier transform. Figure A.2.3 illustrates the different paths used in the UWB/GPS interference measurements, each having their own transfer function. Path AB represents the radiated path, going from the UWB pulse generator to the output of the GPS antenna. Path AC represents the conducted path from the UWB pulse generator to receiver 2, and path AD for receiver 1. Assuming a maximum bandwidth of 24 MHz along each paths, as the signal ultimately passes through the preselector filter of the GPS receiver, we can compare the time-domain response at the output of each path (represented by paths ABF, ACF, and ADF). This is accomplished by multiplying the Fourier transform of the input signal at point A by the transfer function of each component along the chain (whether it be the two antennas, or inline filters) and then performing the inverse Fourier transform on the result. This is done for each of the four paths. Figure A.2.14 shows two pulses: one at the output of the UWB pulse generator and the other at the output of the GPS antenna (via the radiated path). Figure A.2.15 shows the simulated pulses at the output of each of the three paths (ABF, ACF, and ADF). While the pulses at various points along the chain (at different bandwidths) may be quite different, we can see that for the output at the end of each path, when limited in bandwidth by the same 24-MHz filter, there is very little difference in the time-domain characteristics.

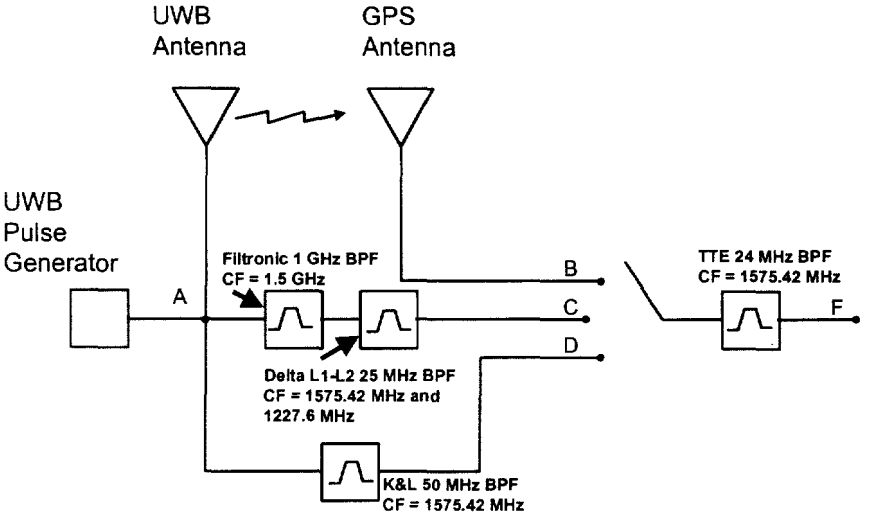

Figure A.2.3. Filter specifications for the different measurement paths.

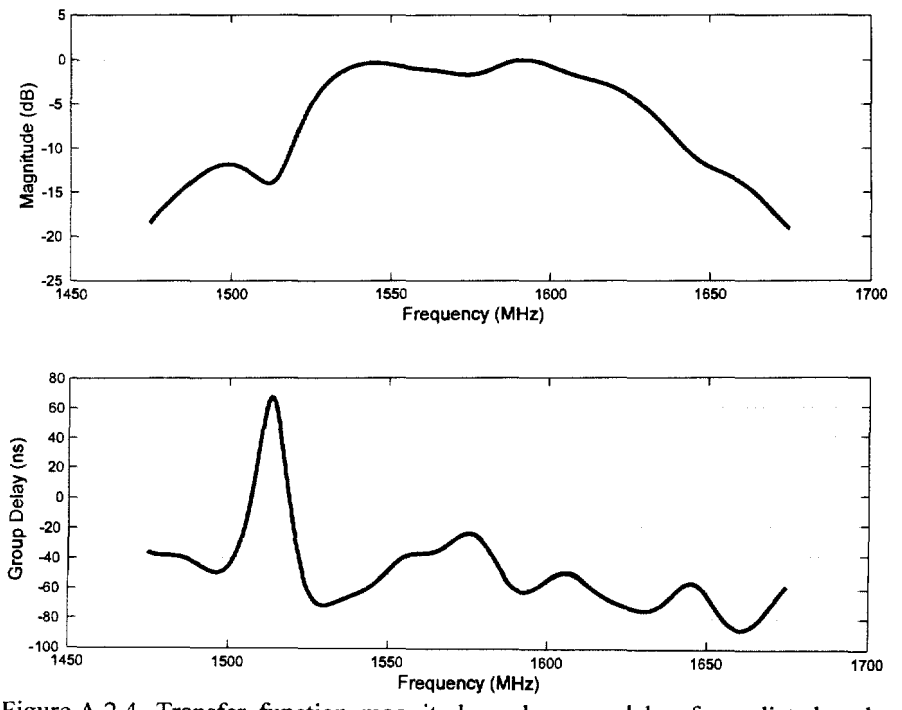

Figure A.2.4. Transfer function magnitude and group delay for radiated path - 1475 MHz to 1675 MHz.

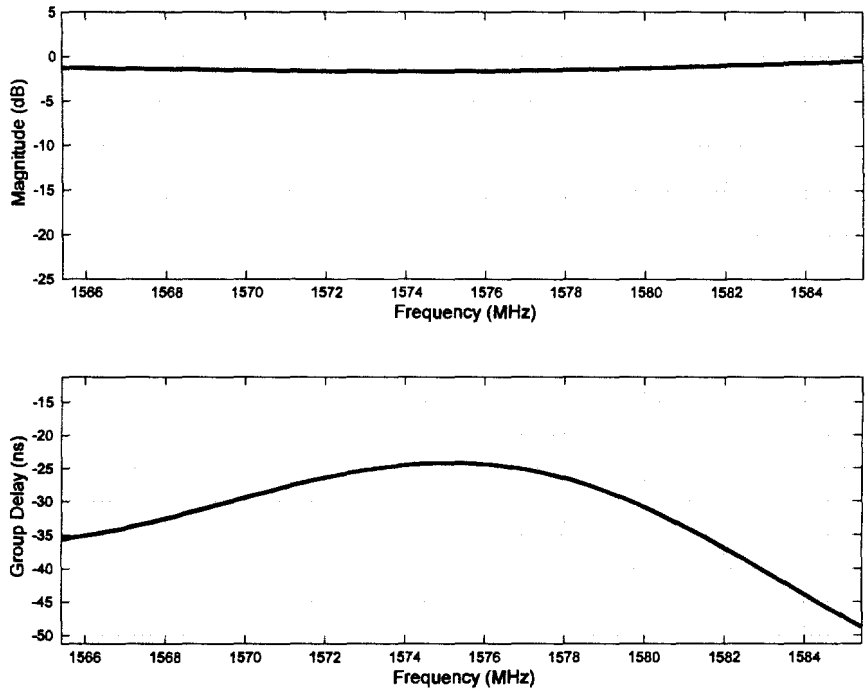

Figure A.2.5. Transfer function magnitude and group delay for radiated path - 1565 MHz to 1585 MHz.

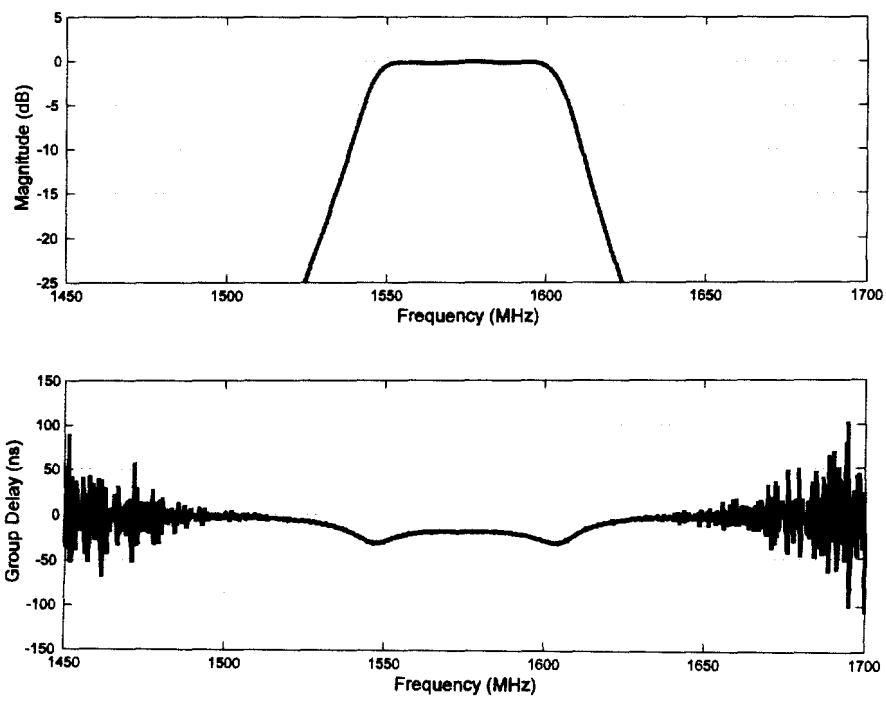

Figure A.2.6. Transfer function magnitude and group delay for filter F3 - 1475 MHz to 1675 MHz.

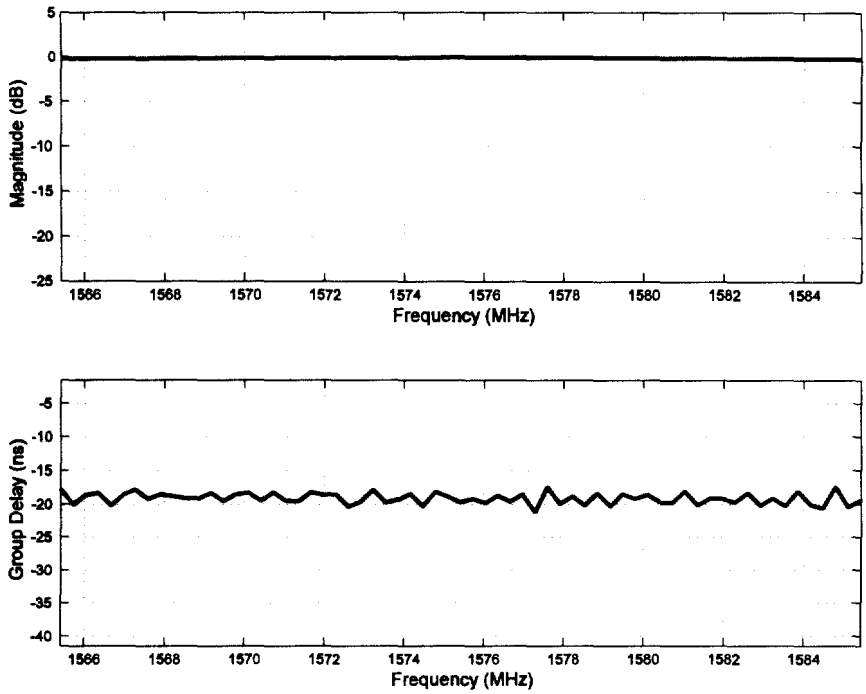

Figure A.2.7. Transfer function magnitude and group delay for filter F3 - 1565 MHz to 1585 MHz.

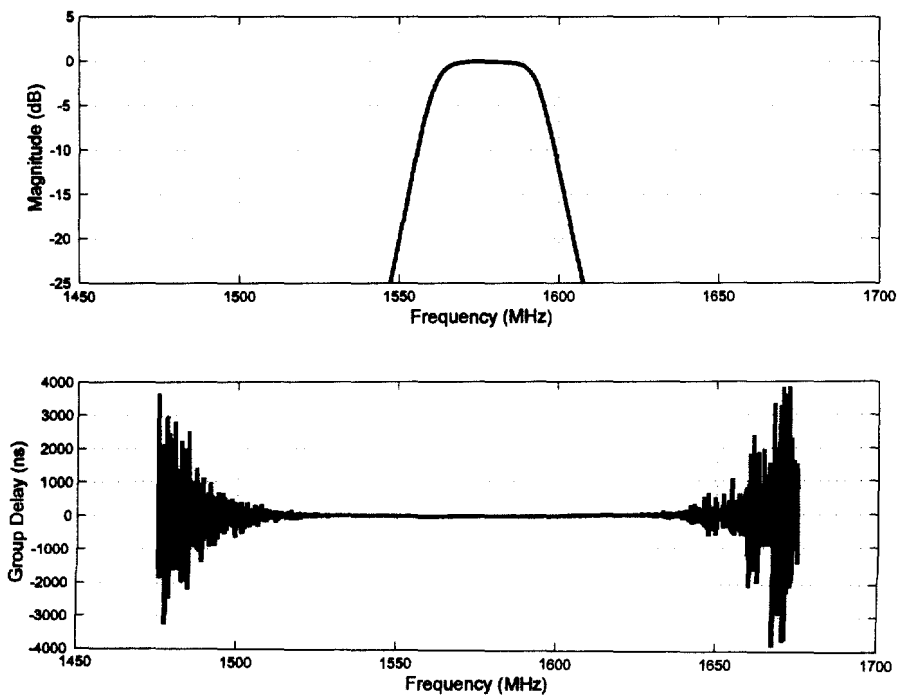

Figure A.2.8. Transfer function magnitude and group delay for filter F1 - 1475 MHz to 1675 MHz.

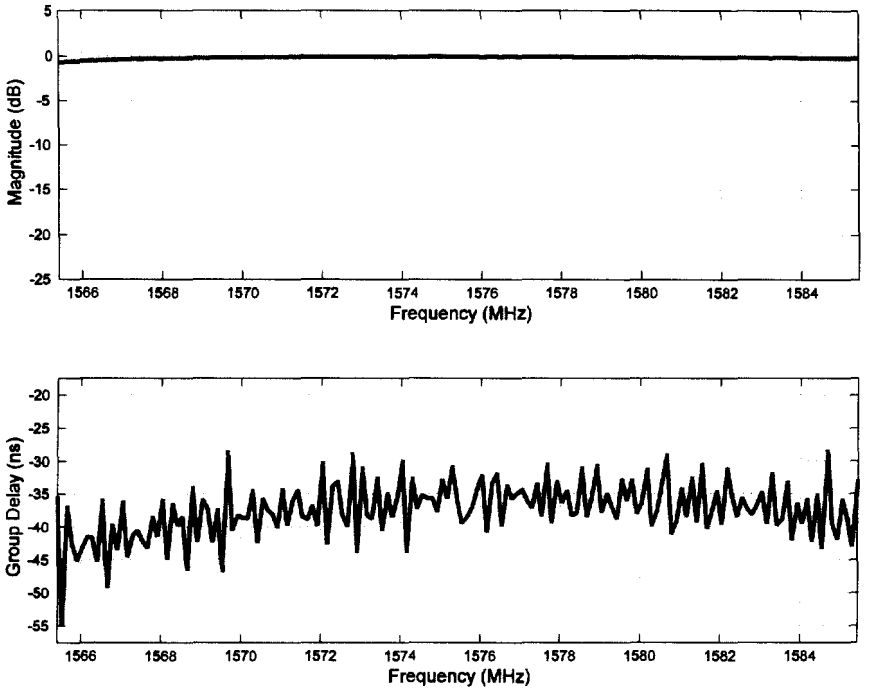

Figure A.2.9. Transfer function magnitude and group delay for filter F1 - 1565 MHz to 1585 MHz.

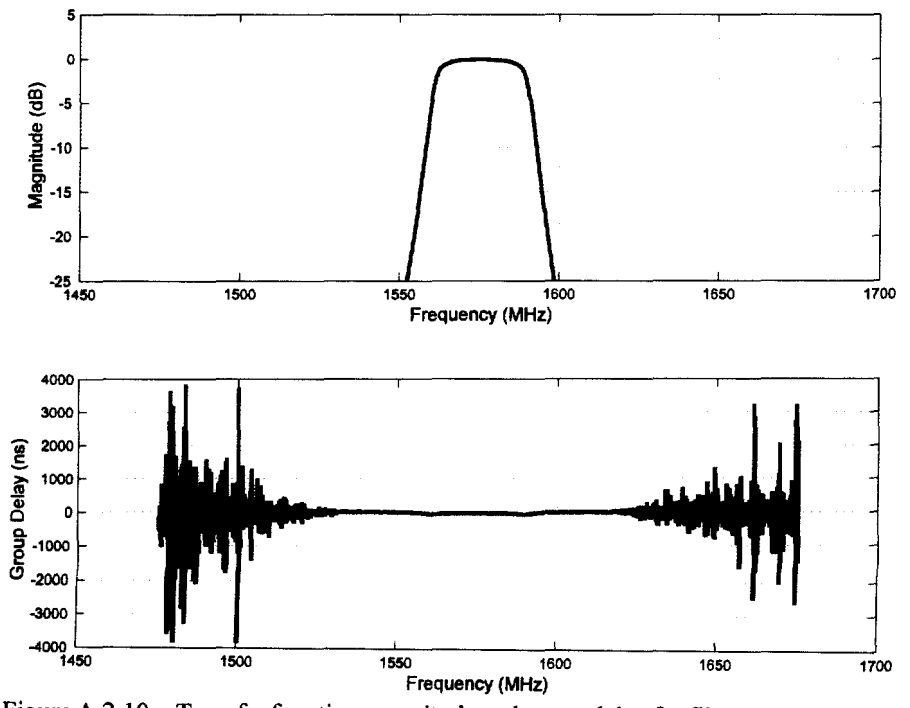

Figure A.2.10. Transfer function magnitude and group delay for filter F4 - 1475 MHz to 1675 MHz.